Applied Energy 335 (2023) 120755

Contents lists available at ScienceDirect

Applied Energy

journal homepage: www.elsevier.com/locate/apenergy

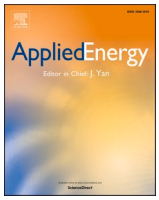

Heat transfer constraints and performance mapping of a closed liquid sorption heat storage process

Benjamin Fumey [a,b,*], Robert Weber [b], Luca Baldini [b,c]

[a] The Lucerne University of Applied Science, School of Engineering and Architecture, Institute of Mechanical Engineering and Energy Technology (IME), Technikumstrasse, 21, 6048 Horw, Switzerland
[b] Empa, Swiss Federal Laboratories for Materials Science and Technology, Überlandstrasse 129, 8600 Dübendorf, Switzerland
[c] ZHAW Zurich University of Applied Sciences, School of Architecture, Design and Civil Engineering, Winterthur, Switzerland

HIGHLIGHTS

- In the sorption heat storage, there is a non-linear relationship between temperature and heat flux, emphasized due to the desired high sorbent concentration gradient.
- This non-linearity brings forth an unavoidable process stagnation when heat at a specific temperature is available but capacity to uptake at the specific temperature is lacking.
- Simple sorption heat storage performance mapping is achieved in a concentration vs gross temperature lift diagram, including equilibrium condition and heat capacity based deviation.

ARTICLE INFO

Keywords:
Liquid sorption heat storage
Sodium hydroxide
Performance evaluation and limitation
Nonlinear temperature to heat correlation
Lab scale demonstrator
Performance mapping

ABSTRACT

Sorption storage is a potential game changer for heat storage in buildings, providing high volumetric energy storage density and no loss over storage time. Application specific temperatures and material specific thermodynamic properties are recognized as key for potential performance evaluation. Nevertheless, in system operation, finite heat and mass transfer kinetics detract from the theoretical maximum performance. In this study, it is found that a nonlinear relationship between temperature gain and heat release of the sorbent, afflicts an unavoidable restriction to the performance potential. Heat transport increases as temperature gain decreases, bringing about a temperature induced heat transfer stagnation to a heat transport fluid with linear temperature to heat gain correlation.

In this paper, we present the background for performance analysis with emphasis on this nonlinear relationship. We propose a method for performance mapping, including the sorbent equilibrium line (the state where the sorbent is in temperature, concentration and vapor pressure equilibrium) and the unavoidable deviation from this line due to the afore stated non-linearity. As an example of this proposed mapping, we visualize results from an absorption process with liquid aqueous sodium hydroxide and water.

Due to the nonlinear temperature rise in heat release, we conclude that it is important to operate a sorption heat storage system in a way that only the minimum required temperature rise is achieved. By doing so, the heat transport fluid capacity is increased in respect to the sorbent capacity, augmenting heat transfer and improving the energy density.

1. Introduction

Thermal energy storage is considered an important prerequisite for the full use of renewable energy in buildings [1–6]. Crucial parameters for success are high energy density, low loss during storage time [7] and low storage cost [8]. Sensible, latent and sorption storage technologies are considered [9]. Sensible and latent storage systems experience continuous heat loss, a major challenge for extended storage periods. This is addressed through large scale sensible storage systems [10] and sub cooling in latent systems [11,12]. Sorption heat storage conversely, basis on a variant of the sorption heat pump with intermittent working

* Corresponding author.
E-mail address: benjamin.fumey@hslu.ch (B. Fumey).

https://doi.org/10.1016/j.apenergy.2023.120755
Received 4 May 2022; Received in revised form 1 January 2023; Accepted 22 January 2023
Available online 7 February 2023

Nomenclature

Abbreviations

c_p	Specific heat capacity [J/(kg K)]
E	Energy [J or kWh]
FR	Flow ratio [-]
GTL	Gross temperature lift
H	Enthalpy [J]
H_2O	Water
HMX	Heat and mass exchanger
HTF	Heat transport fluid
L	Distance [m]
m	Mass [g]
$\dot{m}$	Mass flow [g/min]
NaOH	Sodium hydroxide
P	Power [W]
Q	Heat [J or kWh]
T	Temperature [°C]
ΔT	Change in temperature [K]
V	Volume [m^3]
X	Mass fraction [g/g]

Subscripts

(*)	Lower defined temperature
A	Sorption
a	Sorbent
C	Condensation
D	Desorption
d	Density
E	Evaporation
HTF	Heat transport fluid
in	In
max	Maximum
min	Minimum
out	Out
s	Solution
sens	Sensible
v	Vapor

pair storage [9]. In this way, the potential (work) to recover heat at elevated temperature is stored, rather than storing sensible heat [13]. Major competitive advantages of this approach are potentially high energy density (up to 6 times that of equivalent water-based systems) and no potential loss over time in as far as recombination of the separated media is prevented [7,14]. For this reason, one specific application focused on is inter seasonal heat storage for residential space heating [1,15].

Sorption heat storage follows the concept of a reversible decomposition reaction process. Both thermophysical and thermochemical bonds are included [16,17]. In a bidirectional temperature swing process [18], an aggregate change of the sorbate as a result of evaporation and condensation is incorporated [13,19–24]. Desorption and condensation (charging) and evaporation and sorption (discharging) are separated in time, with the working pair stored in both charged and discharged state [13,25–27]. Processes of adsorption onto solid sorbents [17,28,29] and sorption into solid or liquid sorbents [17,18,25,29,30] are considered. By preventing sorbent and sorbate recombination, the sorption potential can be stored indefinitely, provided the pot life of the material is granted. The solid materials studied include zeolites, silica gels, and salts, as well as the former impregnated with salt, referred to as composite materials. Liquid absorbents studied are usually alkaline aqueous solutions such as sodium hydroxide, calcium chloride, and lithium bromide [31–36]. Generally, water is used as a sorbate because it has a high heat uptake/release in the gas liquid phase change, but generally limits the heat input to temperatures above 0 °C. Other sorbates considered are ethanol and methanol, and ammonia absorbed in water.

There are four different types of processes found in sorption storage systems. These are differentiated into open and closed, and fixed and transported [37]. Open vs closed refers to the contact of the sorbent with the air. Open processes exchange heat and matter (water vapor) with the environment [13,18,38–42], while closed processes are carried out in a vapor atmosphere, generally at sub ambient pressure, and exchange only heat with the environment [13,43–45]. Fixed vs transported refers to the handling of the sorbent. In the fixed process, the sorbent is stationary and connected to the sorber/desorber heat and mass exchanger (HMX) [13,18,34,41,45,46], whereas in the transported process, the sorbent is moved from the storage vessels to the sorber/desorber HMX and back [13,31,34,44,47–49]. Generally, the fixed process is used for solid sorbents and liquid sorbents are transported (pumped). Systems using the transport method have a continuous, uniform power output at a constant temperature, whereas in fixed bed systems this varies greatly depending on the state of charge [37]. Research in this field was started in the early 1960 s [50,51] and is ongoing [52–55], with mature systems yet lacking [56]. In combined tasks of the Solar Heating and Cooling and Energy Storage Technology Collaboration Programs of the International Energy Agency, work has been performed to encourage the overall development and progress performance evaluation, through system categorization [37] and uniform testing guidelines [14]. The investigation in this work contributes to the said line of work by addressing the question of maximum practical system performance in respect to the material based theoretical maximum performance and proceeds to propose an approach to performance mapping.

In this article, we address the issue of unavoidable process limitations in sorption heat storage systems. The work is based on sodium hydroxide (NaOH) and water (H_2O) in a closed transported system, as an example, whereby it is expected that restrictions are applicable for other working pairs and processes. Although, the heat storage sorption process is similar to other heat transformer processes, the concept of storage is unique. High sorbate exchange between working pair charged and discharged state is sought-after, capacitating high energy density. When looking at the system heat release process, the temperature-increase from the low temperature heat source (e.g. ground source heat exchanger) to the heat sink (e.g. building heating system), depends on the sorbent concentration. High concentration warrants high temperature gain. Nevertheless, the mass uptake of sorbate in respect to the mass specific concentration change is not constant. As the concentration decreases and thus temperature gain decreases the mass uptake in respect to concentration change increases. Thus, more heat is available at lower temperature gain. Due to the large concentration gradient, required for high energy density, the non-linearity of temperature gain and heat release of sorbent working pairs is emphasizes. This brings about a stagnation of heat transport from the sorbent to the heat transport fluid with constant temperature dependent heat capacity. This considerable limitation has not been given sufficient attention to. We show that in a diagram displaying concentration vs gross temperature lift, this boundary can be well visualized along with the sorbent equilibrium line. Specific system performance can then be included, providing a simple means of performance mapping.

Focus of this publication is set on pinpointing and calculating said system founded limitation and to propose a method of clear performance mapping. The lab scale results included are provided as an example but not as focal point.

2. Method

2.1. Technical system

This work concerns the closed transported process with the working pair sodium hydroxide (NaOH) and water. The working pair is chosen due to its fitting temperature profile, both in charging and discharging, the high availability of the elements sodium, oxygen and hydrogen as well as the moderate material price in comparison to other liquid sorbents. The technical system employed in this work, consists of two vertically installed spiral finned tubes making up the heat and mass exchanger (HMX) in an interconnected dual chamber as described in [44]. The spiral fins are, 1000 mm long, with a finned length of 900 mm, fin outer diameter of 21 mm, fin width of 4.5 mm, and fin spacing of 2.3 mm. These function as desorber (absorber) and condenser (evaporator) in the charging (discharging) process. Sorbent (sorbate), flows on the tube fin from top to bottom by gravitational force and heat transport fluid (HTF) is pumped from bottom to top through the tube, in counter flow as shown in Fig. 1.

Charging involves a separating process in which heat at elevated temperature is used to evaporate sorbate (in our case H_2O) from the sorbent solution (in our case aqueous NaOH). This vapor is condensed and the heat of condensation is released to the ambient. Concentrated sorbent solution and condensed sorbate are gained and separately stored, preventing recombination (loss of sorption potential). Discharging involves a combining process in which low temperature (ambient) heat is used to evaporate sorbate, which condenses on the charged solution. Since, at equal temperature, the vapor pressure on the solution is lower than the evaporating pressure, the sorbate condenses on the sorbent solution, releasing the heat of condensation. This process continues, increasing the sorbent solution temperature to the point of evaporator to absorber surface pressure equilibrium, deducing a chemically driven heat pump operation with heat released at an elevated temperature.

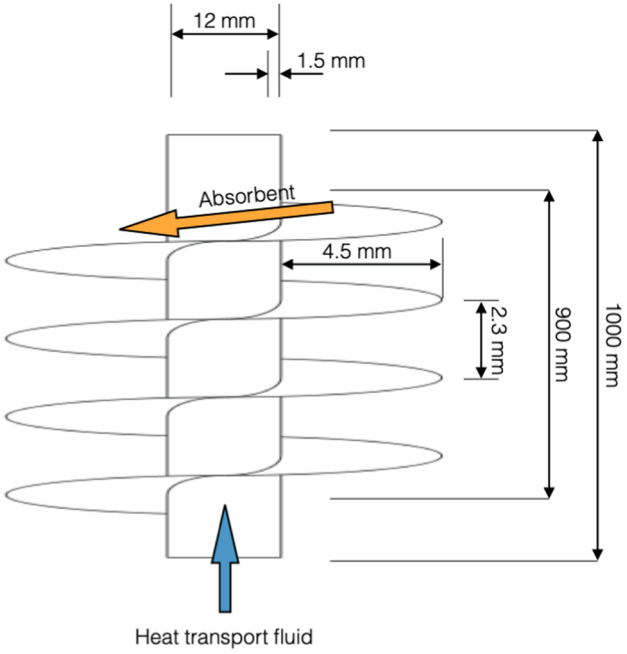

Fig. 1. Illustration of the spiral finned tube. The sorbent flows from top to bottom on the spiral fin and the heat transport fluid is pumped through the inner tube from bottom to top in counter flow.

2.2. Temperature assessment

The operation, and thus also performance, in respect to temperature gain, power and energy density, of a sorption heat storage system is highly dependent on operating temperatures [57]. Source and sink temperatures, both in charging and discharging, are governing [14]. Fig. 2 illustrates the process with particular emphasis on source and sink temperatures in desorption and sorption. Since a temperature swing process is followed, the temperature difference between desorber and condenser in charging and absorber and evaporator in discharging is focal, deriving an increased sorbent concentration in charged state and decreased concentration in discharged state. Energy density basis on its difference, temperature gain on its charged condition, and power on the rate of sorbate mass transport.

For this reason, defining realistic operating (testing) temperatures is a significant initial step in the performance evaluation. Since heat storage for domestic space heating is followed in this work, we find valuable guidance in the electrically driven heat pump testing standard EN 14511 for the discharging (heat release) process [58]. For this work, we consider abidance to existing testing standards to be more universally relevant, rather than to derive own testing conditions from building load simulations. In accordance to the standard, for the evaporator, the heat source supply temperature is 10 °C and the return temperature is 7 °C. The heat sink temperature, for building space heating, is 30 °C supply temperature and 35 °C return temperature. For the charging procedure, we follow the hot water storage tank standard EN12897 [59]. Hereby the maximum heat source supply temperature, for example from solar thermal collectors is 95 °C and by following the EN14511 standard in respect to supply and return temperature difference (3 K), the return temperature is 92 °C. To complete the required temperature profile, condensing conditions need to be defined. These can again be taken from the heat pump standard, whereby heat from air conditioners is released at 30 °C supply temperature and 35 °C return temperature.

From these static temperatures, material temperatures are derived. We take a temperature difference of 2 K, an assumption based on the good thermal conductivity of the liquid sorbent and sorbate and the favorable heat exchange from the counter flow process [60]. This is an average value that is affected by operation and strongly depends on the HMX design. We find that in our standard testing process, the value is well fitting.

The sorbent concentration greatly depends on the temperature difference between the absorber/desorber and the evaporator/condenser. We term this gross temperature lift (GTL). Two variations can be considered, upon basis of the HTF, shown in Table 1 column 4 or in respect to material temperatures, shown in column 6.

In the desorption process, the measure of charged state, in our case the final concentration, is substantially dependent on the GTL. The HTF based GTL is calculated as shown in Eq. (1), based on the desorber and the condenser HTF input temperature. The material GTL considers the temperature difference of the material to the HTL (Eq. (2))

$$GTL_{D_{HTF}} = T_{D_{in}} - T_{C_{in}} \tag{1}$$

$$GTL_{D} = (T_{D_{in}} - 2K) - (T_{C_{out}} + 2K) \tag{2}$$

In the sorption process, the measure if discharge, and thus also the concentration difference between the charged state and the discharged state, which determines the storage energy density, strongly depends on the minimum GTL. The HTF based GTL is calculated as shown in Eq. (3), based on the absorber and evaporator HTF input temperature. The material GTL considers the temperature difference of the material to the HTL (Eq. (4))

$$GTL_{A_{min,HTF}} = T_{A_{in}} - T_{E_{in}} \tag{3}$$

$$GTL_{A_{min}} = (T_{A_{in}} + 2K) - (T_{E_{out}} - 2K) \tag{4}$$

The maximum GTL in the sorption process strongly depends on the

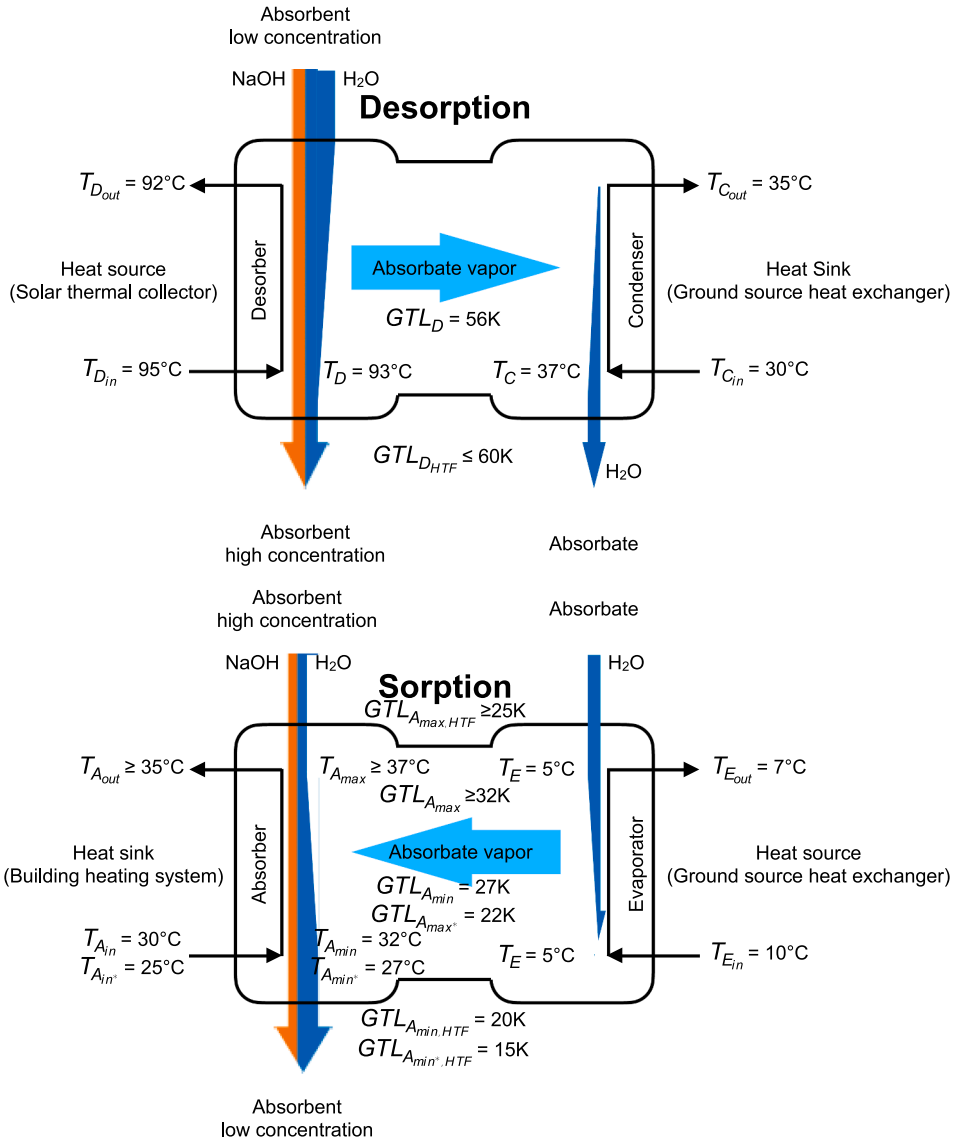

Fig. 2. Illustration of the testing temperature allotment, shown in the desorption (charging) process and sorption (discharging) process. Sorbate release and uptake are illustrated by declining and increasing blue bars. (For interpretation of the references to colour in this figure legend, the reader is referred to the web version of this article.)

Table 1
Operating temperatures for space heating.

Process	Operation	HTF Input Temp.	HTF Output Temp.	HTF GTL	Material Temp.	Material GTL
Discharging	Desorption	$T_{D_{in}} = 95\ °C$	$T_{D_{out}} = 92\ °C$	$GTL_{D_{HTF}} \leq 60\ K$	$T_D = 93\ °C$	$GTL_D \leq 56\ K$
	Condensation	$T_{C_{in}} = 30\ °C$	$T_{C_{out}} = 35\ °C$		$T_C = 37\ °C$	
Charging	Evaporation	$T_{E_{in}} = 10\ °C$	$T_{E_{out}} = 7\ °C$	$GTL_{A_{min,HTF}} = 20\ K$	$T_E = 5\ °C$	$GTL_{A_{min}} = 27\ K$
	Sorption	$T_{A_{in}} = 30\ °C$	$T_{A_{out}} = 35\ °C$		$T_{A_{min}} = 32\ °C$	
				$GTL_{A_{min^*,HTF}} = 15\ K$		$GTL_{A_{min^*}} = 22\ K$
		$T_{A_{in^*}} = 25\ °C$		$GTL_{A_{max,HTF}} \geq 25\ K$	$T_{A_{min^*}} = 27\ °C$	$GTL_{A_{max}} \geq 32\ K$
					$T_{A_{max}} = 37\ °C$	

sorbent starting concentration. The HTF based GTL is calculated based on the absorber HTF output temperature and the evaporator input temperature as shown in Eq. (5). Again, the material GTL considers the temperature difference of the material to the HTL (Eq. (6))

$$GTL_{A_{max,HTF}} = T_{A_{out}} - T_{E_{in}} \tag{5}$$

$$GTL_{A_{max}} = (T_{A_{out}} + 2K) - (T_{E_{in}} - 2K) \tag{6}$$

The material based GTLs are significant for the initial material evaluation and the HTF grounded values for the system evaluation.

For the HTF input temperature ($T_{A_{in}}$), two values are taken to exemplify its importance, 30 °C and 25 °C. The lower value is indicated with an asterisk (*) in the subscript ($T_{A_{in^*}}$). For clarifications sake, the temperatures are illustrated both in the desorption and the sorption process, in Fig. 2.

The sorbent and sorbate temperatures are not strictly defined, but in general storage is taken to be at room temperature (20 °C) or slightly lower. Preventing heat loss from sorbent thermal capacity (e.g. greater

sorbent temperature to storage than from storage) is a matter of system engineering and not addressed in this work.

Founded on the above defined process and temperature profile, an investigation into the expected performance in terms of temperature, power, and energy, is pursued in this work and followed by an evaluation of experimental results as a preliminary example. The initially solely material based investigations, termed 'Material performance' and 'Temperature hysteresis', are followed by considering limitations derived from the HMX process, titled 'Temperature to heat correlation' and 'HMX performance'. This static assessment is complemented by the kinetic evaluation 'Concentration gradient'. From this work, a method of performance mapping is developed and three experimental results are mapped as examples.

3. Results

3.1. Material performance

Initial material evaluation is generally based on the vapor pressure vs temperature diagram with the material equilibrium state presupposed at material temperatures (Table 1, column 5). In our case, the diagram for aqueous NaOH is shown in Fig. 3 with lines drawn to illustrate the charging process (dashed) and the discharging process (full). The referred material temperatures from Table 1 are indicated in brackets. The arrow heads on the vertical lines indicate the process dependency. In desorption (dashed lines) T_C determines the chamber vapor pressure (horizontal line), since operation is under exclusion of non-condensing gases. This in turn defines the maximum concentration, dependent on the maximum sorbent temperature. In sorption (full lines) T_E regulates the chamber vapor pressure and the resulting $T_{A_{max}}$ depends on the sorbent concentration. The final concentration during sorption in discharging depends on $T_{A_{min}}$. In this closed process, the chamber pressure is the temperature-based evaporating / condensing pressure of the sorbate.

In the example (Fig. 3), a concentration of 60 wt% may be reached in charging. Nevertheless, sorbent crystallization beyond 50 wt% at room temperature, limits the charging temperature to 78 °C, noted as T_{D-}, since in our system, sorbent and sorbate are pumped and thus need to remain in liquid state. In discharging, the vapor pressure declines, T_E is substantially lower than T_C, since ambient heat source temperature in winter is lower than in summer. For this reason, $T_{A_{max}}$ is also lower than T_{D-}. The final sorbent concentration in discharged state, and thus also the energy density, depends on the minimum sorbent temperature (space heating return temperature). The energy density (E_d) is calculated based on the water vapor uptake (m_v), and includes the condensing enthalpy (ΔH_v) plus enthalpy of solution (ΔH_s) minus the temperature increase dependent thermal capacity of the condensing water (ΔH_{sens}), divided by the volume of the sorbent and sorbate in charged state (greatest volume, V).

$$E_d = \frac{m_v(\Delta H_v + \Delta H_s - H_{sens})}{V} \quad (7)$$

At $T_{A_{min}}$ ($T_{A_{min^*}}$), the sorbent concentration is 42 wt% (38 wt%), and the energy density, based on the sorbent volume in its discharged state, 160 kWh/m^3 (227 kWh/m^3). Precise temperature assessment is thus very important.

The material based GTLs in desorption and sorption are indicated in Fig. 3, for further clarification of the values.

3.2. Temperature hysteresis

In Fig. 3 it can be recognized that at a fixed vapor pressure, the GTL depends on the sorbent concentration. Alternative visualization of process can be obtained by plotting sorbent concentration in respect to changing GTL. This diagram is derived from Fig. 3 by changing the specific temperature to the temperature difference (GTL) at a fixed vapor pressure, plotted to the specific resulting concentration. Fig. 4 shows this plot with two lines representing material-based equilibrium conditions in charging (T_C) and discharging (T_E). In reading the diagram, discrete temperatures can be obtained by adding the vapor pressure equivalent temperature (T_C or T_E) to the x-axis value and energy density is asserted based on the concentration change visible on the y-axis.

In this representation, a temperature hysteresis is recognized, not clearly visible in the scope of Fig. 3. The effect is based on the changing vapor pressure. At T_C the GTL to reach 50 wt% is 41 K and at T_E it is 38 K. Thus, a decline in GTL of 3 K occurs between the charging and discharging processes. Furthermore, this hysteresis affects energy density. Where 42 wt% concentration and from this 160 kWh/m^3 are reached with T_E, and 40.5 wt% and 200 kWh/m^3 are achieved in the case of T_C at equal minimum GTL. The lower evaporating temperature in discharging thus negatively affects both the maximum output temperature and the energy density. This is a consequence of the application as heat storage, since classically in this application $T_C \geq T_E$.

In our work, this concentration vs GTL diagram provides the basis for simple performance mapping and will be adhered to. In technical operation, desorption results are always to the right of the equilibrium state ($P1$), in horizontal deviation from equilibrium, since temperature and thus pressure imbalance is required to remove sorbate. Operational values for sorption are always to the left of the equilibrium state ($P2$) since imbalance is again required for uptake of sorbate. Difference in GTL is represented by horizontal (temperature) deviation from

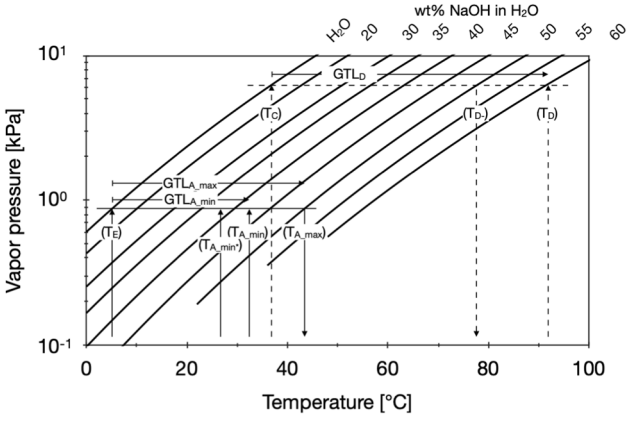

Fig. 3. Vapor pressure vs temperature diagram of NaOH. Indicated is the process based on the proposed operating values.

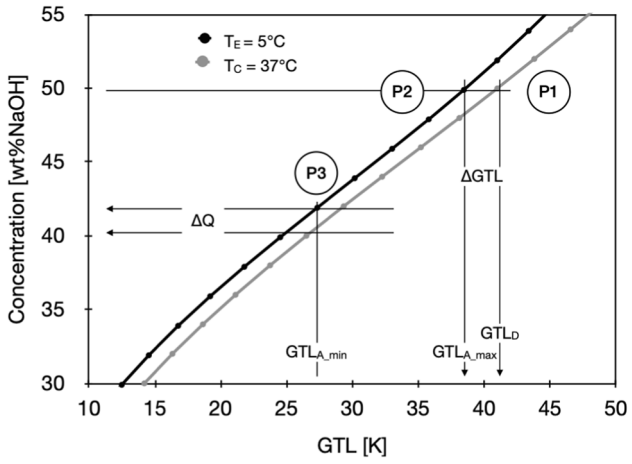

Fig. 4. Diagram showing concentration vs GTL of aqueous NaOH at T_E and T_C equivalent vapor pressures. Indicated are the vapor pressure dependent GTL and capacity losses. Technical operating points $P1$ (required charging GTL), $P2$ (resulting discharging GTL), and $P3$ (resulting final concentration) are included.

equilibrium and concentration in vertical deviation (*P*3).

3.3. Temperature to heat correlation

As noted in the previous chapter, GTL at constant vapor pressure, depends on sorbent concentration. In contrast to this, heat release from sorption is a function of the water vapor uptake. In the progression of desorption (sorption), the amount of water vapor released (taken up) in respect to the concentration change, decreases (increases), see Eq. (8). In the equation, X is the mass fraction and m_{H_2O} is the water mass in the solution in respect to the NaOH mass. If the mass fraction (X) is 0.5 (50 wt%) then the solution contains equal mass of water and NaOH, if it is 0.25 (25 wt%) then the water mass is 3 times that of the NaOH mass. Thus, while the mass fraction change, effecting GTL is linear, the change of water content, energy transport, is not.

$$m_{H_2O} = \frac{1}{X} - 1 \tag{8}$$

Consequently, the correlation between sorbent temperature and released heat (vapor exchange) is not linear, while the HTF heat capacity is, based on the assumption of constant specific heat. This imposes limitations on heat transfer from sorbent to HTF in discharging. The issue is illustrated in the temperature vs heat diagram in Fig. 5. Desorption is not affected, since in this case the sorbent line (black with dots) curves to the overlaying HTF line (dotted) and ends can meet, allowing maximum heat transport. Contrastingly, in sorption the sorbent line curves away from the lower positioned HTF line, permitting only a single point of contact, restricting heat flux. Thus, while the HTF thermal capacity can be altered dependent on the mass flow, linearity remains. Three variations of HTF flow are shown in the diagram. At low flow, the maximum HTF temperature is reached but energy transfer (capacity) is curbed due to the increase in sorbent heat release at lower temperatures and the coherent lack of HTF thermal capacity, and vice versa at high HTF flow. Energy density and temperature are therefore inter-linked and the thermal capacity of the HTF (flow) influences the specific potential of a sorption storage system. This issue arises from the broad spectrum of concentration and is expected to applies to all sorption heat storage concepts and materials.

These limitations can be included in the concentration vs GTL diagram of Fig. 4. To specify the capacity balance, an HTF to sorbent mass flow ratio (FR) is used.

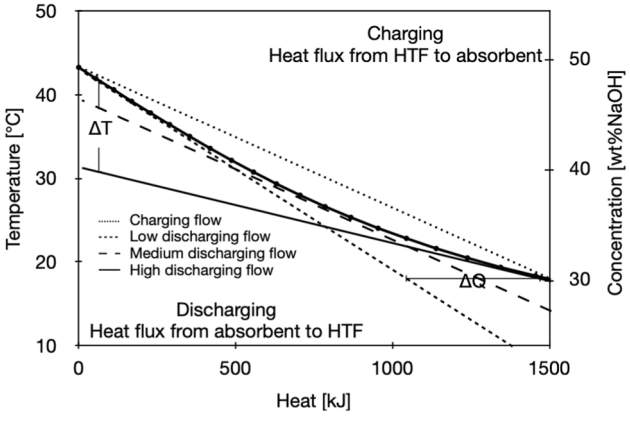

Fig. 5. The diagram shows the principle of heat transfer in the HMX. The black dotted downwards bent line shows the heat released, for 1 kg of charged aqueous NaOH at a starting concentration of 50 wt%, and a saturated water vapor pressure at T_E. The dotted line above the black curve illustrates the constant HTF thermal capacity during charging. The dashed and full lines below the curve illustrate varying HTF capacities (flows) during discharging with only a single contact, showing the resulting temperature and/or capacity loss. The y-axis on the right indicates the respective sorbent solution concentration change.

$$FR = \frac{\dot{m}_{HTF}}{\dot{m}_a} \tag{9}$$

Depending on the FR, more or less heat can be transferred by the HTF. If the sorbent heat capacity surpasses that of the HTF, the HTF reaches the sorbent temperature, but the sorbate uptake is restricted reducing the achieved energy density (Eq. (10)). In the case where the heat capacity of the sorbent equals that of the HTF (point of line contact), the HTF temperature equals the sorbent temperature and maximum sorbate uptake is attained (Eq. (11)). Finally, if the HTF capacity exceeds that of the sorbent, maximum sorbate uptake is arrived at, but the HTF temperature does not reach the sorbent temperate (Eq. (12)).

$$if(\Delta Q_a > \Delta Q_{HTF}) then(T_{HTF} = T_a) and(m_{H_2O_{uptake}} < m_{H_2O_{max}}) \tag{10}$$

$$if(\Delta Q_a = \Delta Q_{HTF}) then(T_{HTF} = T_a) and(m_{H_2O_{uptake}} = m_{H_2O_{max}}) \tag{11}$$

$$if(\Delta Q_a < \Delta Q_{HTF}) then(T_{HTF} < T_a) and(m_{H_2O_{uptake}} = m_{H_2O_{max}}) \tag{12}$$

In Fig. 6, performance curves at FRs of 8 to 16 are shown. At a FR of 8, the curve touches the equilibrium line at 50 wt%. This means that the maximum temperature is arrived at. Since the curve deviates from the equilibrium at lower concentration, this points to the lack of HTF thermal capacity and thus hindrance for maximum discharge, afflicting capacity loss. Considering $T_{A_{min}}$ ($T_{A_{min^*}}$) the final concentration increases from 42 wt% to 43 wt% (38 wt% to 40 wt%), bringing about an energy density drop from 160 kWh/m^3 to 142 kWh/m^3 (227 kWh/m^3 to 195 kWh/m^3). With a FR of 12 (14), the minimum concentration for $T_{A_{min}}$ ($T_{A_{min^*}}$) is arrived at, maximizing energy density, at the toll of 1.8 K (4.2 K) output temperature decline.

Up to this point in the evaluation, the focus has been on temperature and energy. Based on the FR, initial evaluation of power, the most complex parameter amidst the trio, can now be approached. By multiplying the HTF specific heat capacity (c_p), its temperature increase (ΔT_A) and the FR, a value of power (P) per sorbent mass flow ($\dot{m}_a$) with the unit J/kg or in our case more conveniently W/(g/min) is derived. This is a specific power value, from which an absolute power value can be attained by multiplication with the specific sorbent mass flow. The sorbent mass flow is in reference to the supply flow, in sorption being of 50 wt% concentration. It must be noted that this does not involve the uptake of sorbate. This must be so, since the uptake of sorbate and the respective change of sorbate concentration, flow and heat capacity is directly dependent on the operating temperature and the HMX design.

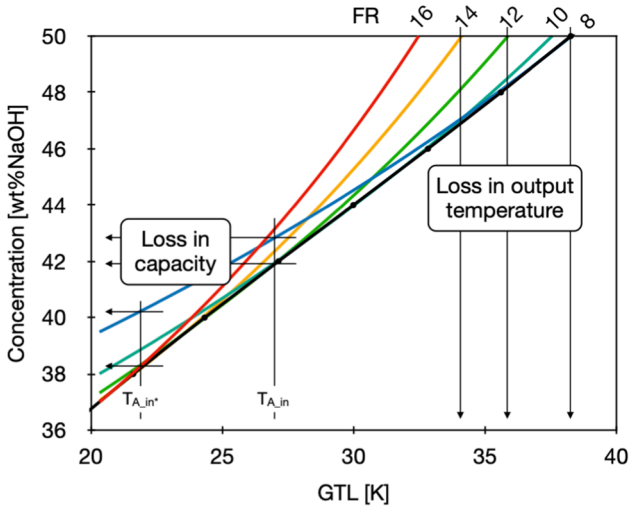

Fig. 6. Diagram showing concentration vs GTL at T_E. Included are calculated flow ratio (FR) curves of 8 to 16. Deviation from the equilibrium curve indicates temperature decline and storage capacity loss.

$$\Delta T_A = \Delta T_{A_{out}} - T_{A_{in}} \tag{13}$$

$$\frac{P}{\dot{m}_a} = c_p \Delta T_A FR \tag{14}$$

Looking at the previous example in Fig. 6, at the FR of 8, representing a low HFT thermal capacity, the power per sorbent flow ($\frac{P}{\dot{m}_a}$) also decreases, since maximum sorbent exploitation (sorbate uptake) is hindered. It thus results that at a FR of 8, $\frac{P}{\dot{m}_a}$ is 9 W/(g/min) and at 16 it is 12.8 W/(g/min). Thus, the nonlinear temperature to heat correlation additionally interlinks temperature and power.

3.4. HMX performance

Up to this point, our considerations on performance evaluation are based on sorption material temperatures (Table 1, column 6 and 7). On a system scale, the HTF temperatures are consequential and we propose that these are to be taken as basis for the performance evaluation diagram. In sorption, equilibrium thus depends on $T_{E_{in}}$, a value greater than T_E.

In Fig. 7, performance (temperature, power and energy density) is compared dependent on varying temperature profiles. All temperatures are taken from Table 1:

1. Ideal: Assuming no temperature decline on the HMX ($T_{E_{in}}$, $T_{A_{in^*}}$, $T_{A_{out}}$).
2. Realistic ($T_{A_{min^*}}$): Including temperature decline on the HMX (T_E, $T_{A_{min^*}}$, $T_{A_{max}}$).
3. Realistic ($T_{A_{min}}$): Including temperature decline on the HMX (T_E, $T_{A_{min}}$, $T_{A_{max}}$).

Condition (1) assumes an evaporating temperature of 10 °C ($T_{E_{in}}$), a $GTL_{A_{min^*,HTF}}$ of 15 K, and requires a $GTL_{A_{max,HTF}}$ of 25 K to reach 35 °C output temperature ($T_{A_{out}}$). This is achieved with a FR of 32, granting maximum discharge to a final concentration of 32 wt% and an energy density of 308 kWh/m^3 at a relative power of 22.4 W/(g/min).

Condition (2) includes HMX heat transfer-based temperature decline, T_E is 5 °C, and $T_{A_{min^*}}$ is 27 °C. The minimum GTL is now 22 K ($GTL_{A_{min^*}}$) and a GTL of 32 K ($GTL_{A_{max}}$), is required to reach a $T_{A_{max}}$ of 37 °C allowing 35 °C output temperature ($T_{A_{out}}$). Under these conditions, the FR reduces to 18, the final concentration increases to 38 wt%, the energy density reduces to 227 kWh/m^3, and the relative power is 12.7 W/(g/min).

Under condition (3), the absorber HTF input temperature is increased to 30 °C ($T_{A_{in}}$), increasing the minimum GTL to 27 K ($GTL_{A_{min}}$), while keeping the required GTL to reach 35 °C output temperature at 32 K ($GTL_{A_{max}}$). Under these conditions, the FR increases to 22.5, the final concentration increases to 42 wt%, and the energy density decreases to 160 kWh/m^3. Even though the FR is greater under condition (3) compared to condition (2), the relative power reduces to 7.8 W/(g/min) since the absorber HFT temperature difference is reduced.

Thus, power and energy performance are closely interlinked and substantially dependent on temperature conditions.

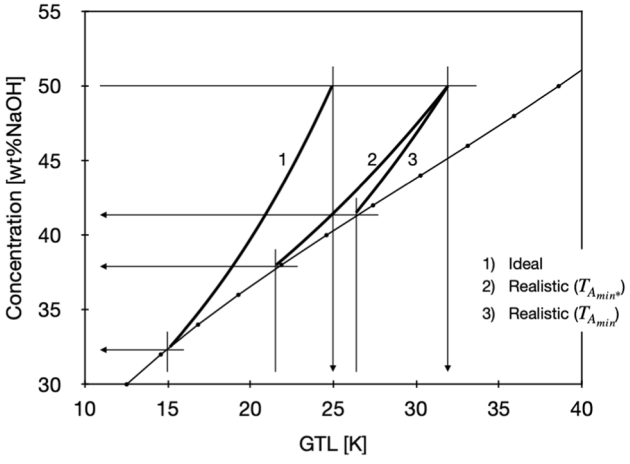

Fig. 7. Concentration vs GTL diagram showing the evaluation of performance based on the three conditions; 1) Ideal, 2) Realistic ($T_{A_{min^*}}$), and 3) Realistic ($T_{A_{min}}$). Lines with arrows are included to indicate GTL and concentration values. The arrows indicate the evaluation direction.

3.5. Concentration gradient

So far, material equilibrium conditions have been assumed with temperature decline on the HMX accounted for. In technical operation, additional, material-based mass and heat transport limitations are encountered. These are heavily dependent on the heat and mass exchanger design. To understand the basic mass transport response, a study of water vapor uptake and mass transport into static aqueous sodium hydroxide thin films under relevant temperatures was performed, using temporally and spatially resolved Raman spectroscopy [60].

Fig. 8 shows that particularly in the sorption process (centered in the diagram), the rate of sorbate uptake (power) is highly concentration dependent and leads to a concentration gradient in the thin film. It is also shown that the film depth increases as the sorbate content increases. Long exposure times, due to spatial and temporal gradients, are required to reach close to equilibrium concentration at the end of the sorption and desorption process. For this reason, even though the transported process enables a constant system output power, Fig. 8 shows that, as the concentration throughout the length of the HMX decreases, much time is required for water vapor uptake and heat release to reach low (close to equilibrium) concentration and with-it high-energy density. Thus, the average area and volume specific power of a sorption storage HMX will be substantially lower compared to the sorption process in a chiller or heat pump with small concentration differences across the HMX.

3.6. Experimental testing results

Three sorption tests with varying sorbent flow (2 g/min, 4 g/min,

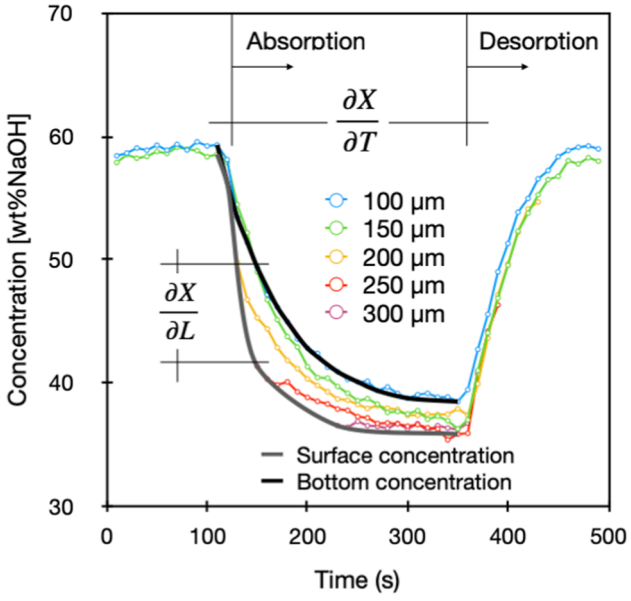

Fig. 8. Spatially and temporally resolved NaOH concentration measured operando during water sorption and desorption, at a temperature of 35 °C and 55 °C, respectively, and constant evaporating temperature of 5 °C. Indicated are both the spatial (∂X/∂L) and the temporal (∂X/∂T) gradient. The measuring depth of the varying curves is indicated.

and 6 g/min) are performed using our single tube lab test bench [44] see Table 2. The FR is kept constant at 25, with an absorber HTF flow of 50 g/min, 100 g/min, and 150 g/min respectively. HTF temperatures as defined in Table 1 are applied, whereby $T_{A_{min^*}}$ is taken. $GTL_{A_{max\,HTF}}$ is derived from $T_{A_{out}}$ minus $T_{E_{in}}$ (Eq.5). Results are mapped in the concentration vs GTL diagram in Fig. 9, compared to the ideal performance under the defined conditions, calculated to be; 27.8 K GTL, 22.3 W/(g/min) power, and 308 kWh/m^3 energy density based on equations 10–12, 14, and 7. Included are the equilibrium curve at 10 °C evaporating temperature and the ideal performance curve at the FR of 25.

The results and comparison of the three different test cases show clearly that for a fixed FR, at higher sorbent mass flows the actual potential of the sorbent solution in terms of energy storage capacity and temperature lift is not fully exploited. Specific power decreases along with the energy density and the output GTL. This is due to the limitations in mass and heat transfer kinetics. Mass flow increase at equal HMX surface leads to an increase in film depth and greater flow. While the later reduces the exposure time of the sorbent to the sorbate vapor, increased film depth increases the mass transport distance from the condensing surface of the sorbent to the sorbent film bulk, see Fig. 8, increasing the concentration gradient. For this reason, more time is required to approach equilibrium condition (decline of gradient and temperature specific concentration). The increased mass flow rate on the HMX counteracts this requirement and both lead to a reduction in energy density and sorbent flow relative power. For this reason, as shown in Fig. 9, at constant FR, output temperature, relative power and energy density decrease as sorbent flow increases. A sorbent system will thus be designed for a nominal temperature gain, power and energy density, based on a defined operating temperature profile (Table 1).

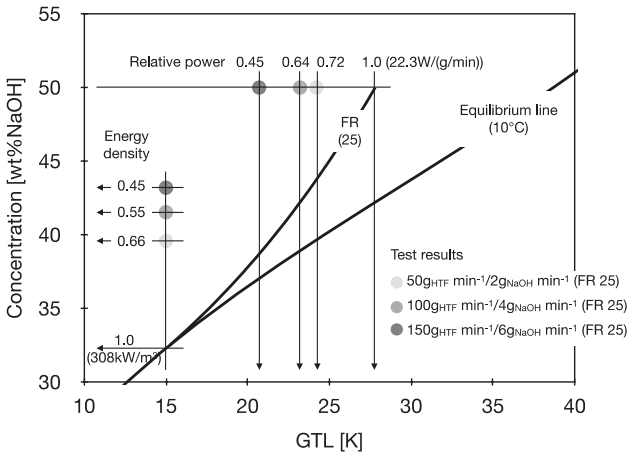

Fig. 9. Concentration vs GTL diagram including FR dependent curves and lab scale HMX test results.

4. Discussion

In this paper, a careful look at the closed and transported liquid sorption process is undertaken in light of the long-term heat storage application. A fundamental challenge is found.

We propose that the three basic parameters for the sorption heat storage performance evaluation, as would be central for any heat storage system, are; the system output temperature ($T_{A_{out}}$), the charge/discharge power, and the volumetric energy density. In a technical system, failure to reach the required output temperature and power, deem the system nonfunctional. The parameter unique to the sorption storage application, in comparison to the sorption heat pump, is energy density. Sorption heat pumps and chiller follow a continuous process of desorption and absorption, without sorbent capacity storage. The question arises, what this novel criterion brings about in respect to operation limitations.

It is argued that a pragmatic, application specific HTF input and output temperature profile is at the root of clear operation evaluation. Comparison between different systems as well as system evaluation such as cycling stability can only be performed if a uniform constant temperature profile is applied. We propose a profile based on heat pump testing standards, since the sorption heat storage functions as a chemically driven heat pump. We believe that this will be more globally accepted than own results from building load simulation and encourage other researchers in the field to follow, making comparison possible. From the HTF supply and return temperatures, material temperatures derive. These are central for an initial material evaluation. As illustrated, it would be wrong to take the HTF temperatures for the material evaluation, since temperature difference between sorbent and sorbate to HTF is inevitable. In our example with liquid sorbent and counter flow heat exchange, we take an average difference of 2 K. This is low, compared to solid sorbents in packed bed reactors with high thermal resistance. The temperature difference between heat supply and sink, termed “gross temperature lift” or GTL, is an important value strongly effecting final concentration both in desorption and absorption and thus also energy density. Based on the GTL and the concentration, we derive a method for simple performance mapping. In this diagram, operational points based on concentration and GTL can be visualized and compared to theoretical maxima, or to varying test results.

Founded on the temperature profile, a stepwise discourse on the operational potential, from preliminary material performance and temperature hysteresis to the nonlinear temperature to heat correlation and concentration gradient is followed. These steps are taken to evaluate the practical performance potential upon which technical results may be assessed.

We show that, since inclusion of energy capacity broadens the concentration scope of function, additional operation limitations derive. This is founded on the nonlinear temperature to heat correlation (section 3.3). The desorption process is not affected, since starting and ending conditions meet (Fig. 5), and, in our case, approaching final charging concentration (heat and mass transport kinetics) can be accelerated by increasing GTL_{D-} (Fig. 3), since the required charging temperate is generally below the maximum available. Contrarily, in the sorption process, the restriction applied, and careful assessment of the theoretical potential is necessary to perform a clear technical evaluation to assert the specific HMX design. For this reason, the absorption process is now further discussed.

Absorption as also desorption, both depend on the evaporator/condenser temperature, which defines the vapor pressure in the HMX chamber. For this reason, the sorbent equilibrium line, the state at which the sorbent is in temperature and concentration equilibrium at a specific vapor pressure equivalent temperature is central. In terms of temperature and energy density, derived from the concentration difference, this is the absolute theoretical maximum. We propose, that the equilibrium line used in the performance mapping basis on the HTF temperature. It is

Table 2
Test results from a lab scale sorption storage heat pump.

Test #	Sorbent Flow [g/min]	$GTL_{A\_max\_HTF}$ [K]	Power [W]	Sorbent flow relative Power		Energy density	
				[W/(g/min)]	Relation to max. (22.3)	[kWh/m^3]	Relation to max. (308)
1	2	24.2	32.0	16.0	0.72	202.5	0.66
2	4	23.2	57.2	14.3	0.64	170.4	0.55
3	6	20.7	59.6	9.9	0.45	139.9	0.45

clear that the material values will divert from this due to temperature loss in heat transfer. Nevertheless, exactly this temperature loss is part of the accumulated performance decline. In our application (example), the evaporator supply temperature is taken to be 10 °C ($T_{E_{in}}$). In our performance mapping, the equilibrium line at 10 °C is therefore included. If $T_{E_{in}}$ changes, the equilibrium line adjusts respectively. The second and third consequential temperatures are $T_{A_{in}}$ ($T_{A_{in^*}}$) and $T_{A_{out}}$, in our case 30 °C (25 °C) and 35 °C. Based on these temperatures and therefrom resulting specific FR, a second curve is added to the diagram, showing the performance decline due to the nonlinear temperature to heat correlation (Fig. 7). This is the practicable maximum performance. From this, the maximum relative power is also derived (Equation (14)), completing the performance trio. Again, if $T_{A_{in}}$ and $T_{A_{out}}$ divert from the defined values, the curve is adapted, adjusting the relative power and energy density. The performance evaluation of a system thus basis on the diversion from this practicable maximum curve. By mapping this on the concentration vs GTL diagram, simple visualization is reached.

While in operation, the testing conditions are unalterable, either following the temperature profile in Table 1 or in a real setting fixed by the heat source (ground source heat exchanger) and sink (building), the sorbent flow ($\dot{m}_a$) and the HTF flow (or FR) are alterable parameters, jointly impacting power output. Upon this, two evaluation schemes are obtained:

Scheme 1) variable $\dot{m}_a$, sequel FR, and fixed $T_{A_{out}}$: In this approach, the FR is adjusted to reach a fixed $T_{A_{out}}$ based on $\dot{m}_a$ which is flexible, affecting the specific power output. The changing values are power and energy density. The specific power can then be divided by $\dot{m}_a$ to derive the sorbent mass flow relative power, a value that can be compared at varying specific power settings.

Scheme 2) variable $\dot{m}_a$, fixed FR: In this approach, the FR is kept constant and only $\dot{m}_a$ is changed, affecting specific output power. The changing values in this case are $T_{A_{out}}$, power, and energy density. Again, the sorbent mass flow relative power can be calculated for comparison of varying tests.

Setting 1 is the application true assessment since the required $T_{A_{out}}$ is upheld and thus true relative power and energy density are verified for $\dot{m}_a$. Version 2 on the other hand can provide insight into influencing limitations. By keeping the FR constant, the increase in power in respect to $\dot{m}_a$ theoretically remain linear under ideal conditions, resulting in constant mass flow related power, energy density and $T_{A_{out}}$. Diversion there from points to process resistance and design limitations. This differs to scheme 1, where due to the change in the FR, required to uphold $T_{A_{out}}$, since operation is not ideal, final theoretical energy density changes.

Looking at the provided testing example, under ideal conditions, at a FR of 25 and a $GTL_{A_{min^*,HTF}}$ of 15 K, a $GTL_{A_{max,HTF}}$ of 27.8 K, a power output of 22.3 W/(g/min), and an energy density of 308 kW/m^3 (32 wt%) are calculated. These are the maximum values under the defined conditions and the evaluation basis. In Fig. 9, the performance mapping of the three example results is shown. The diagram includes both the theoretical maximum (equilibrium line) and the practicable maximum (FR limitation line). The concentration and GTL maximum values are noted as unit, with specific values in brackets. The three test results are plotted showing the maximum GTL at 50 wt% concentration and the final concentration at $GTL_{A_{min^*,HTF}}$ (15 K), extended with the fraction of relative power and energy density. In this way, Fig. 9 provides a straightforward overview of the performance parameters $T_{A_{out}}$ ($T_{E_{in}} + GTL$), relative power, and energy density at varying specific power output. It is seen that at increased power output (higher sorbent and HTF flow) at constant FR, the performance to the theoretical maximum declines. Test 1, at the lowest specific power, has the highest relative power and energy density. Even so, there is a diversion from the maximum. This is expected, maximum cannot be reached in practice due to limited thermal and mass transport kinetics. Chapter 3.5 shows mass transport restrictions. Again, these are more severe in the absorption process than in desorption. Increase in mass flow at constant absorber area leads to an increase in film depth and flow. Greater film depth requires longer time for sorbate mass transport from the film surface to the film bulk and concentration gradient increases. Greater mass flow on the other hand reduces the sorbent exposure time. For this reason, both the sorbent mass flow relative power as well as the energy density are reduced.

The performance mapping clearly visualizes the working limits of a respective HMX component. In-depth evaluation is now possible based on more detailed measurement. By measuring the actual evaporating temperature on the evaporator, a second FR limitation line can be drawn, showing the loss of performance due to the temperature drop on the evaporator. Again, by measuring the maximum and minimum sorbent temperature on the absorber, this can also be included. In this way overall evaluation can be segmented and the varying individual contributions quantified.

In our testing example, it is clear that mass transport of sorbate into sorbent is limiting, since temperature differences of the HTF to the sorbent and sorbate only marginally increase as $\dot{m}_a$ is increased. Technical design challenges are thus at hand to increase the mass transport kinetics.

5. Conclusion and outlook

In this paper we pursue a method for sorption heat storage performance mapping. Central for this mapping (evaluation) is the derivation of the technical maximum. We show that this is not the equilibrium condition, but diverts there from due to the concentration based nonlinear temperature to heat correlation. Based on this we argue that both maximum temperature and energy density as suggested in the equilibrium evaluation cannot be achieved, indifferent of heat and mass transport kinetic. In the transported liquid sorbent process the flow ratio (FR) of sorbent to heat transport fluid (HTF) provides a good method for determining the potential output temperature, power and energy density, recognized as the three main heat storage performance parameters. Diversion from this technical maximum, points to kinetic limitations from heat and mass transport, showing potential for heat and mass exchanger (HMX) improvement.

Visual mapping is achieved by plotting specific test results in respect to the FR maximum in the concentration vs GTL diagram. In order to evaluate the degree of individual performance hindrance in heat and mass transport, additional curves can be included based on local temperature and pressure measurements on the HMXs. For example, based on the actual evaporation temperature, being lower than the evaporator input temperature ($T_{E_{in}} < T_E$) a second FR curve can be added, showing the share of performance decline due to the evaporator temperature reduction. Based on the findings in this work, a more precise evaluation of performance is possible, since unavoidable limitations are observed. This enables to better detect and eliminate (reduce) design-based bottle necks. From this evaluation, it is recognized that, in order to achieve the best performance, the FR should be chosen such that the minimum required output temperature is reached, permitting respective application specific maximum discharging, enabling maximum power and maximum energy density.

Funding

This work was supported by the Swiss Innovation Agency Innosuisse in the frame of the Swiss Competence Centre for Energy Research Heat and Electricity Storage (SCCER HaE), grant Nr. 1,155,002,545 and the Swiss Federal Office of Energy SFOE grant Nr. SI/501605–01.

CRediT authorship contribution statement

Benjamin Fumey: Conceptualization, Methodology, Investigation, Writing – original draft, Visualization. **Robert Weber:** Conceptualization, Writing – review & editing. **Luca Baldini:** Writing – review &

editing, Supervision, Project administration, Funding acquisition.

Declaration of Competing Interest

The authors declare that they have no known competing financial interests or personal relationships that could have appeared to influence the work reported in this paper.

Data availability

Data will be made available on request.

References

[1] Wang R, Zhai X. Handbook of energy systems in green buildings. ISBN978-3-662-49185-0. Springer-Verlag Berlin Heidelberg; 2018.
[2] International Energy Agency Solar Heating and Cooling Programme (IEA SHC). Task 58. Advanced thermal storages - towards higher energy densities, long term storage and broader operating ranges. 2018. p. 12–4.
[3] Stutz B, Le Pierres N, Kuznik F, Johannes K, Barrio EPD, B ́ed ́ecarrats J-P, et al. Storage of thermal solar energy. Comptes Rendus Phys 2017;18:401–14. https://doi.org/10.1016/j.crhy.2017.09.008.
[4] Baldini L, Fumey B. Seasonal Energy Flexibility Through Integration of Liquid Sorption Storage in Buildings. Energies 2020;13:2944.
[5] van Helden W, Yamaha M, Rathgeber Ch, Hauer A, Huaylla F, Le Pierrès N, et al. IEA SHC task 42/ ECES Annex 29 – working group B: applications of compact thermal energy storage. Energy proced 2016;91:231–45.
[6] International Energy Agency. Energy technology perspectives report. 2016978-92-64-25233-2.
[7] Hadorn JC. IEA solar heating and cooling programme—task 32: advanced storage concepts for solar and low energy buildings. Proceedings of ECO- STOCK. 2006.
[8] Rathgeber Ch, Hiebler S, Lävemann E, Dolado P, Lazaro A, de Gasia J, et al. IEA SHC task 42/ECES Annex 29 – a simple tool for the economic evaluation of thermal energy storages. Energy Procedia 2016;91:197–206.
[9] Tatsidjodoung PL, Pierrès N, Luo L. A review of potential materials for thermal energy storage in building applications. Renew Sustain Energy Rev 2013;18:327–49.
[10] Kabus F, Wolfgramm M. Aquifer thermal energy storage in Neubrandenburg -Monitoring throughout three years of regular operation. EFFSTOCK'2009. In: 11th International Conference on Thermal Energy Storage, Stockholm, Sweden; 2009.
[11] Dannemand MJ, Kong JB, Furbo W, S.. Experimental in- vestigations on cylindrical latent heat storage units with sodium acetate trihydrate composites utilizing supercooling. Appl Energy 2016;177:591–601.
[12] Englmair G, Moser Ch, Furbo S, Dannemand M, Fan J. Design and functionality of a segmented heat-storage prototype utilizing stable supercooling of sodium acetate trihydrate in a solar heating system. Appl Energy 2018;221:522–34.
[13] Zondag, HA. Chapter 6 - Sorption Heat Storage, Editor(s): Bent Sørensen, Solar Energy Storage, Academic Press; 2015. p. 135–54.
[14] Fumey B, Baldini L. Static Temperature Guideline for Comparative Testing of Sorption Heat Storage Systems for Building Application. Energies 2021;14:3754. https://doi.org/10.3390/en14133754.
[15] Haghighat F. Energy storage with energy efficient buildings and districts: optimization and automation. Tech Rep. 2018.
[16] Vasiliev LL, Kulakov AG. Heat Pipe Applications in Sorption Re- frigerators. In: Kakaç S., Smirnov H.F., Avelino M.R. (eds) Low Tempera- ture and Cryogenic Refrigeration. NATO Science Series (Series II: Mathe- matics, Physics and Chemistry), vol 99. Springer, Dordrecht; 2003.
[17] Inglezakis VJ, Poulopoulos S. Adsorption, ion exchange and catalysis: design of operations and environmental applications. Elsevier; 2006.
[18] Perry RH. Perry's chemical engineers' handbook. eighth ed. Mc Grawhill; 2007.
[19] Garg HPM, Bhargava SC, Ak.. Solar thermal energy storage. Dordrecht: Reidel Publishing Company; 1985.
[20] Kawasaki H, Watanabe T, Kanzawa A. Proposal of a chemical heat pump with paraldehyde depolymerization for cooling system. Applied Thermal Energy 1999;19(2):133–43.
[21] Boman BDH, Staedter DC, Goyal MA, Ponkala A, Garimella MJ, S.. A method for comparison of absorption heat pump working pairs. Int J Refrig 2017;77:149–75.
[22] Aristov YI. Challenging offers of material science for adsorption heat transformation: a review. Appl Therm Eng 2013;50(2):1610–8.
[23] N'Tsoukpoe KEL, Pierrès N, Luo L. Experimentation of a LiBr- H2O absorption process for long-term solar thermal storage: prototype design and first results. Energy 2013;53:179–98.
[24] Cabeza LFS, Barreneche A, C.. Review on sorption materials and technologies for heat pumps and thermal energy storage. Renew Energy 2017;110:3–39.
[25] Hauer A. Sorption theory for thermal energy storage. In: Paksoy HÖ, editor. Thermal energy storage for sustainable energy consumption. Netherlands: Springer; 2007. p. 393–408.
[26] Bales, C. (2005). Thermal Properties of Materials for Thermo-chemical Stor- age of Solar Heat. A Report of IEA Solar Heating and Cooling programme – Task. 32. 2005.
[27] Kato Y. Chemical energy conversion technologies for efficient energy use. Netherlands: Thermal energy storage for sustainable energy consumption. Springer; 2007. p. 377–91.
[28] Wang LWW, Oliveira RZ, Rg.. A review on adsorption working pairs for refrigeration. Renew Sustain Energy Rev 2009;13(3):518–34.
[29] Srivastava NCE, Iw.. A review of adsorbents and adsorbates in solid- vapour adsorption heat pump systems. Applied Thermal Engi- neering 1998;18(9–10):707–14.
[30] Armstrong F, Blundell K. Energy beyond oil. Oxford University Press; 2007.
[31] N'Tsoukpoe KE, Liu H, Le Pierrès N, Luo L. A review on long-term sorption solar energy storage. Renew Sustain Energy Rev 2009;13(9):2385–96.
[32] Kuznik F, Johannes K, Obrecht Ch, David D. A review on recent developments in physisorption thermal energy storage for building applications. Renew Sustain Energy Rev 2018;94:576–86.
[33] Palomba V, Frazzica A. Recent advancements in sorption technology for solar thermal energy storage applications. Sol Energy 2018. in press.
[34] Solé A, Martorell I, Cabeza LF. State of the art on gas–solid thermochemical energy storage systems and reactors for building applications. Renew Sustain Energy Rev 2015;47:386–98.
[35] Yu N, Wang RZ, Wang LW. Sorption thermal storage for solar energy. Prog Energy Combust 2013;39:489–514.
[36] Abedin AH, Rosen MA. A critical review of thermochemical energy storage systems. Open Renew Energy J 2011;4:42–6.
[37] Fumey B, Weber R, Baldini L. Sorption based long-term thermal energy storage – Process classification and analysis of performance limitations: A review. Renew Sustain Energy Rev 2019;111:57–74.
[38] Zondag H, Kikkert B, Smeding S, de Boer R, Bakker M. Prototype thermochemical heat storage with open reactor system. Appl Energy 2013;109:360–5.
[39] Kerskes H, Mette B, Bertsch F, Asenbeck S, Drück H. Development of a thermo-chemical energy storage for solar thermal applications. Proceedings of ISES solar world congress. 2011.
[40] Weber R, Asenbeck S, Kerskes H, Drück H. SolSpaces – testing and performance analysis of a segmented sorption store for solar thermal space heating. Energy proced 2016;91:250–8.
[41] van Alebeek R, Scapino L, Beving MAJM, Gaeini M, Rindt CCM, Zondag HA. Investigation of a household-scale open sorption energy storage system based on the zeolite 13X/water reacting pair. Appl Therm Eng 2018;139:325–33.
[42] Tatsidjodoung P, Le Pierrès N, Heintz J, Lagre D, Luo L, Durier F. Experimental and numerical investigations of a zeolite 13X/water reactor for solar heat storage in buildings. Energy Convers Manag 2016;108:488–500.
[43] Weber R, Dorer V. Long-term heat storage with NaOH. Vacuum 2008;82(7):708–16.
[44] Fumey B, Weber R, Baldini L. Liquid sorption heat storage – A proof of concept based on lab measurements with a novel spiral fined heat and mass exchanger design. Appl Energy 2017;200:215–25.
[45] Köll R, van Helden W, Engel G, Wagner W, Dang B, Jänchen J, et al. Experimental Investigation of a realistic scale seasonal solar sorption storage system for buildings. Sol Energy 2017;155:388–97.
[46] Zondag H, Kalbasenka A, van Essen M. First studies in reactor concepts for thermochemical storage. Proceedings of the Eurosun 2008.
[47] Mette B, Kerskes H, Drück H. New high efficient regeneration process for thermo-chemical energy stores. Proceedings of innostock 2012.
[48] Boman DB, Hoysall DC, Pahinkar DG, Ponkala MJ, Garimella S. Screening of working pairs for adsorption heat pumps based on thermodynamic and transport characteristics. Appl Therm Eng 2017;123:422–34.
[49] Mette B, Kerskes H, Drück H. Concepts of long-term thermochemical energy storage for solar thermal applications – selected examples. Energy proced 2012;30:321–30.
[50] Goldstein M. Some physical chemical aspects of heat storage. In: UN Conf. New Sources Energy, Rome (Italy); 1961. http://digitallibrary.un.org/recor d/3828050. [Accessed 19 December 2020].
[51] Goldstein M. Some physical chemical aspeets of heat storage: Goldstein, Martin, United National Conference on new sources of energy, Rome, 1961, 17 p., Sol Energy 7 (2) (1963) 84. doi:10.1016/0038-092X(63)90029-X.
[52] International Energy Agency, Solar Heating and Cooling Programm, Task 42: https://task32.iea-shc.org.
[53] International Energy Agency, Solar Heating and Cooling Programm, Task 42: https://task42.iea- shc.org.
[54] International Energy Agency, Solar Heating and Cooling Programm, Task 58: https://task58.iea- shc.org.
[55] International Energy Agency, Solar Heating and Cooling Programm, Task 67: https://task67.iea- shc.org.
[56] Kokouvi Edem N'Tsoukpoe. Frederic Kuznik, A reality check on long-term thermochemical heat storage for household applications. Renew Sustain Energy Rev 2021;139:110683.
[57] Boman DB, Hoysall DC, Staedter MA, Goyal A, Ponkala MJ, Garimella S. A method for comparison of absorption heat pump working pairs. Int J Refrig 2017;77:149–75.
[58] EN 14511. Air Conditioners, Liquid Chilling Packages and Heat Pumps with Electrically Driven Compressors for Space Heating and Cooling—Part 2: Test Conditions. Available online: https://www.en-standard.eu/din-en-14511-2-air-conditioners-liquid- chilling-packages-and-heat-pumps-for-space-heating-and-coo

ling-and-process-chillers-with-electrically-driven-compressors- part-2-test-conditions/.
[59] EN 12897. Water Supply—Specification for Indirectly Heated Unvented (Closed) Storage Water Heaters. Available on- line: https://www.en-standard.eu/din-en-12897-water-supply-specification-for-indirectly-heated-unvented-closed-storage- water-heaters-includes-amendment-2020/ (accessed on 8 May 2021).
[60] Fumey B, Baldini L, Borgschulte A. Water Transport in Aqueous Sodium Hydroxide Films for Liquid Sorption Heat Storage. Energy Technol 2020;8:2000187.